ACS APPLIED MATERIALS & INTERFACES

Research Article

www.acsami.org

# Magnetic and Electrical Transport Properties of $LaBaCo_2O_{5.5+\delta}$ Thin Films on Vicinal (001) $SrTiO_3$ Surfaces

Chunrui Ma, Ming Liu, Gregory Collins, Haibin Wang, Shanyong Bao, Xing Xu, Erik Enriquez, and Chonglin Chen*

Department of Physics and Astronomy, University of Texas at San Antonio, Texas 78249, United States

Yuan Lin

State Key Laboratory of Electronic Thin Films and Integrated Devices, University of Electronic Science and Technology of China, Chengdu, Sichuan 610054, People's Republic of China

Myung-Hwan Whangbo

Department of Chemistry, North Carolina State University, Raleigh, North Carolina 27695-8204, United States

**ABSTRACT:** Highly epitaxial $LaBaCo_2O_{5.5+\delta}$ thin films were grown on the vicinal (001) $SrTiO_3$ substrates with miscut angles of 0.5°, 3.0°, and 5.0° to systemically study strain effect on its physical properties. The electronic transport properties and magnetic behaviors of these films are strongly dependent on the miscut angles. With increasing the miscut angle, the transport property of the film changes from semiconducting to semimetallic, which results most probably from the locally strained domains induced by the surface step terraces. In addition, a very large magnetoresistance (34% at 60 K) was achieved for the 0.5°-miscut film, which is ~30% larger than that for the film grown on the regular (001) $SrTiO_3$ substrates.

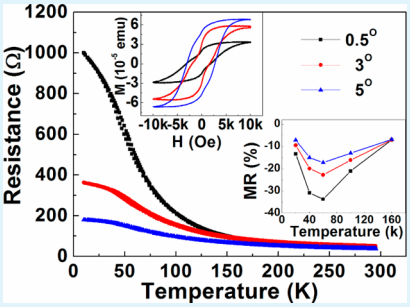


**KEYWORDS:** *epitaxial thin film, $LaBaCo_2O_{5.5+\delta}$, magnetoresistance, surface and interface, vicinal surface, electronic transport*

## INTRODUCTION

Epitaxial thin films of perovskite oxides have many important applications in the development of novel-concept devices, since they exhibit a very wide range of electrical, magnetic, and optical properties. In the perovskite oxide family, cobalt perovskites doped with alkaline-earth (AE) elements at the A-site, $(Ln,AE)CoO_3$ (Ln = lanthanide, AE = Ca, Sr, or Ba), are most attractive, because of their high-temperature mixed electronic/ionic conduction as well as their electrical and magnetic properties for energy-harvesting device development and potential novel-concept device applications,[1−9] which include read/write heads in magnetic data storage, oxidation catalysts, gas sensors, and energy harvest and conversion devices. There are two types of A-site doped cobalt perovskites, namely, A-site disordered and A-site ordered structures, which are dependent on the size of the AE cation and the synthesis conditions.[10,11] The A-site ordered structure is favorable when the cation size difference between the Ln and AE ions is large. The A-site disordered structure is formed when the cation size difference is small. Therefore, it is difficult for $(La,Ba)CoO_3$ to form an A-site ordered structure because the size difference between $La^{3+}$ and $Ba^{2+}$ ions is not large. Recently, systematical studies indicated that the A-site ordered double-perovskite structure, $LaBaCo_2O_{5.5+\delta}$ (LaBCO), can be achieved under a special treatment at high temperature and high pressure.[10−12] To fully understand the physical phenomena in this complex system, it is critical to prepare single crystalline LaBCO samples.

Recently, we have successfully fabricated highly epitaxial LaBCO thin films with A-site ordered and nanoscale ordered structures on different single crystalline substrates and observed that they possess various interesting physical properties.[13−16] A large magnetoresistance (MR) effect (19%) was observed for the LaBCO films grown on (001) $SrTiO_3$, and a much greater MR effect (54%) for those grown on (001) MgO.[17] These results indicate that the interface strain in the highly epitaxial LaBCO thin films can significantly alter the physical properties of the films such as low-temperature magnetization, MR,[16,18] and high-temperature electrical transport properties.[14,15] Besides strain generated from the lattice misfit between the substrate and the LaBCO film, the substrate surface structures such as surface step, terrace, kink sites as well as other defect distribution are also important factors affecting the microstructures and the physical properties of the films.[19−24] To

Received: November 2, 2012
Accepted: December 27, 2012
Published: December 27, 2012

  

further understand the effects of the surface step-terrace on the physical properties, we have systematically investigated the magnetic and electrical transport properties of highly epitaxial LaBCO thin film on the vicinal (001) $SrTiO_3$ substrates with different miscut angles (0.5°, 3.0°, and 5.0°) along the [110] axis and observed various interesting electronic transport properties and anomalous magnetic phenomena.

## EXPERIMENTAL SECTION

A KrF excimer pulsed laser deposition system with a wavelength of 248 nm was employed for the LaBCO thin film growth on the vicinal (001) $SrTiO_3$ substrates with miscut angles 0.5°, 3.0°, and 5.0°. To prepare the substrate surfaces with $TiO_2$ surface termination, the as-received vicinal (001) $SrTiO_3$ substrates were annealed at 875 °C in a 200 Torr pure oxygen environment, which is known to guarantee the pure $TiO_2$ surface termination.[25] The optimal growth condition for achieving highly epitaxial LaBCO films was found to be at 850 °C under an oxygen pressure of 250 mTorr and the laser energy density of 2.0 J/cm$^2$ in a repetition rate of 5 Hz. The as-grown LaBCO thin films were then post-annealed at 850 °C for 15 min in a pure oxygen pressure of 200 Torr before cooling them slowly to room temperature at a rate of 5 °C/min. The crystallinity and epitaxial behavior of the LaBCO films were examined using a high-resolution X-ray diffraction (XRD). The electrical transport and magnetic properties of the as-grown LaBCO films were systematically studied using a Quantum Design Physics Property measurement system (Model PPMS-9).

## RESULTS AND DISCUSSION

Figure 1 shows the typical XRD $\theta$–$2\theta$ scans of the as-grown LaBCO films on the vicinal (001) $SrTiO_3$ with the miscut

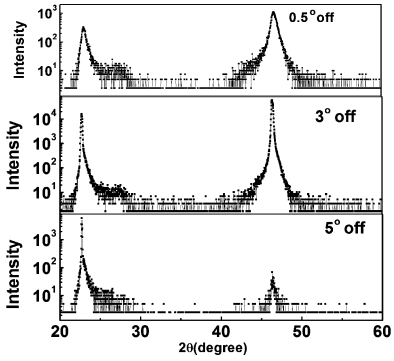


**Figure 1.** Typical X-ray diffraction (XRD) spectra of the epitaxial LaBCO films grown on the vicinal (001) $SrTiO_3$ substrate with miscut angles of 0.5°, 3.0°, and 5.0°.

angles 0.5°, 3.0°, and 5.0°. Similar to the epitaxial growth of LaBCO films on the regular (001) $SrTiO_3$ substrates, only the ($h$00) peaks appear, suggesting that the as-grown films are $a$-axis-oriented. The ($h$00) film peaks are superimposed on the substrate peaks due to the very small lattice constant difference between the substrate ($a_s$ = 0.3905 nm) and the film ($a_f$ = $b_f$ = 0.3886 nm, $c_f$ = 0.7716 nm). The reciprocal space measurements were conducted to examine the epitaxial quality and interface strain distributions. The $\theta$–$2\theta$ contour plot shows that the full width at half-maximum (FWHM) from all as-grown films has a value comparable to that from the substrates, as can be seen in Figure 2, suggesting excellent single crystallinity and epitaxial nature of the as-grown films.

The magnetic and electrical transport property measurements were conducted using a PPMS-9 system at various temperatures under different applied magnetic fields. Figure 3 shows the temperature dependence of electrical resistance of

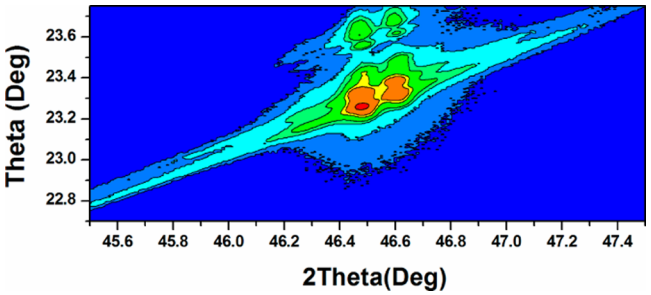


**Figure 2.** Typical reciprocal space mapping of the epitaxial LaBCO thin film grown on the vicinal (001) $SrTiO_3$ (miscut angle = 0.5°).

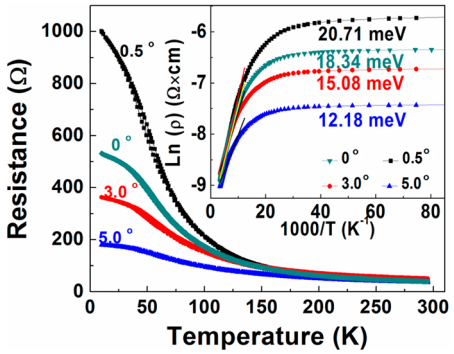


**Figure 3.** Temperature dependence of the resistance (from 300 K to 20 K) for the as-grown LaBCO thin films on the vicinal (001) $SrTiO_3$ substrate with different miscut angles. The inset shows the Arrhenius plot of the resistivity ($\rho$) versus inverse temperature ($T^{-1}$) and the activation energy ($E$) calculated from the thermal activation hopping model.

the LaBCO films on various vicinal (001) $SrTiO_3$ substrates. The resistivity ($\rho$) of the LaBCO films decreases rapidly as the miscut angles of the vicinal (001) $SrTiO_3$ substrates increase. Obviously, at low temperatures, the resistance curve is neither the traditional semiconductor behavior, that the resistance increases exponentially with decreasing temperature, nor metallic behavior, that the resistance normally decreases with decreasing temperature. Instead, all the films show semiconductor to semimetallic behavior with very complicated transport mechanisms (typically called "dirty semimetallic" behavior[26,27]), which are similar to that from the bulk LaBCO material.[28] The electronic transport behavior of LaBCO thin films on these vicinal (001) $SrTiO_3$ substrates were also studied by the thermal activation model, or ln $\rho \propto 1/T$, near the room temperature region, as seen in the inset of Figure 3. The activation energies of the LaBCO films were derived to be 21, 15, and 12 meV, respectively, from the linear regions of the Arrhenius plots. These values are very close to that from the reported bulk value of 21 meV[29] but smaller than the value reported for $GdBaCo_2O_{5.5}$.[30,31] Isothermal MR measurements were performed for the as-grown LBCO films as a function of magnetic field ($H$) between 0 and 7 T, as seen in Figure 4. Here, MR (%) = $[\rho(H) - \rho(0)]/\rho(0) \times 100\%$. The MR of the LaBCO on the 0.5° miscut (001) $SrTiO_3$ is much larger than those on the other two miscut substrates, reaching the maximum value of ~34% at 60 K, which is much greater than the maximum value of 15% found for its bulk material at 10 K[11] or the maximum value of 24% for the films grown on the regular (001) $SrTiO_3$.[16] Figure 5 is the temperature dependence of the field-cooled (FC) (under 0.05 T)


dx.doi.org/10.1021/am302553y | ACS Appl. Mater. Interfaces 2013, 5, 451–455

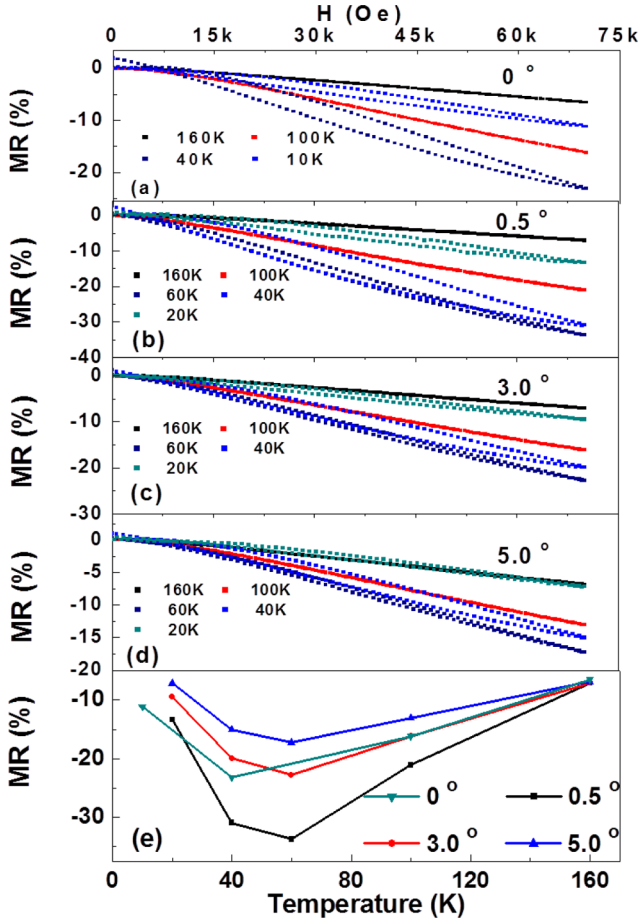


**Figure 4.** Magnetoresistance (MR) versus the magnetic field at different temperature and the temperature dependence of the MR of the as-grown LaBCO MR films under a magnetic field of 7 T.

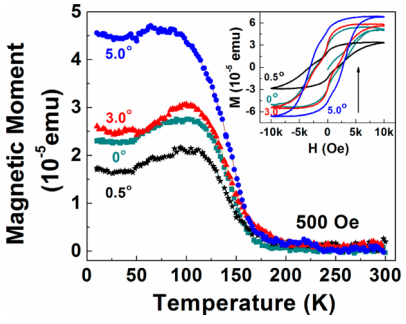


**Figure 5.** Temperature dependence of the magnetization of the FC epitaxial LaBCO film grown on the vicinal (001) $SrTiO_3$ substrates with various miscut angles. The inset shows the magnetization hysteresis loop of the as-grown LaBCO thin film at 30 K.

magnetization measurements for these LaBCO films. Two transitions occur during the temperature scan between 10 K and 300 K; the first is observed at ~50 K and the other is observed at 170 K. The ~170 K transition is associated with the change from the paramagnetic (PM) state to a ferromagnetic (FM) state, and the ~50 K transition is associated with the change from the FM to an antiferromagnetic (AFM) state. A nonzero magnetic moment until 10 K indicates that the FM and AFM states coexist in the films, which can also be confirmed by a hysteresis loop at 30 K shown in the inset of Figure 5, as reported earlier.[12,29]

To understand the nature of these anomalous physical phenomena, we systematically investigated the local strain of the thin films on various miscut (001) $SrTiO_3$ substrates. The miscut (001) $SrTiO_3$ substrate surfaces usually consist of various arrays of steps and terraces, depending on the miscut angles. Normally, the (001) $SrTiO_3$ surface consists of surface terraces of various sizes with each step height of one unit cell. Table 1 summarizes the average widths of the substrate terraces as well as how many unit cells of the substrates and those of the films on the terraces are estimated as listed in Table 1.

**Table 1. Average Width of the Substrate Terrace in the Epitaxial LaBCO Thin Films Grown on the Vicinal (001) $SrTiO_3$, and the Numbers of Unit Cells of the Substrate $SrTiO_3$ and LaBCO ($n_s$ and $n_f$, respectively) That the Average Terrace Can Accommodate**

| miscut angle | terrace width (nm) | $n_s$ | $n_f$ |
|---|---|---|---|
| 0.5° | 44.748 | 114.6 | 115.16 |
| 3.0° | 7.458 | 19.1 | 19.2 |
| 5.0° | 4.474 | 11.46 | 11.52 |

For the LaBCO thin films on the 0.5°, 3.0°, and 5.0° miscut (001) surfaces of $SrTiO_3$, the average widths of the substrate terrace widths are estimated to be 44.748, 7.458, and 4.474 nm, respectively (see Table 1). The number of unit cells of the substrate $SrTiO_3$ and LaBCO ($n_s$ and $n_f$, respectively) that the average terrace can accommodate are summarized in Table 1. For the thin films grown on the 3.0° and 5.0° miscut substrates, the $n_s$ and $n_f$ differ very slightly (only 0.10 and 0.06 unit cell difference, respectively), suggesting that the local strain from the surface step is very small. Moreover, when the miscut angle is larger, the terrace width is narrower, which is smaller than the mean characteristic surface diffusion length of the surface atoms at the growth temperature.[32,33] Therefore, as the miscut angle of the vicinal (001) $SrTiO_3$ substrate increases, the film growth will follow the step-flow mechanism, resulting in the single domain formation.[34] The single-domain growth and small lattice-misfit strain will reduce the scattering of conduction electrons, which leads to a smaller resistance than does the film grown on the regular (001) $SrTiO_3$ substrate (i.e., misfit angle 0°). For the thin film grown on the 0.5° miscut substrate, the difference between $n_s$ and $n_f$ is ~0.5 unit cells. This thin-film/substrate mismatch (i.e., the residual mismatching) will result in an additional strain energy and will be stored in the heteroepitaxial films. As the film continues to grow away from the substrate surface, the strain energy induced by residual mismatching will accumulate in the heteroepitaxial film. Unlike metal or semiconductor thin films, the oxide thin film growth requires a good match in the combination of positive and negative charge balance, because of ionic bonding of the oxide films. Thus, when a number of film unit cells fill up along the terrace, a mismatch gap can be generated at the end of the step terrace (i.e., the "residual mismatching gap"), as seen in Figure 6a. Practically, this residual mismatching gap will not exist at the end of the step terrace in an epitaxial film. The last atomic plane of the film will always occupy the atomic position of the terrace end by rearranging the local atomic structure. Thus, two possible atomic rearrangements for the highly epitaxial oxide thin films can be considered: the formation of nonconservative antiphase domain boundary[20] and that of the locally strained domain induced from the "residual mismatching gap", as seen in Figures 6b and 6c. For the 0.5 unit cell residual mismatching


dx.doi.org/10.1021/am302553y | ACS Appl. Mater. Interfaces 2013, 5, 451−455

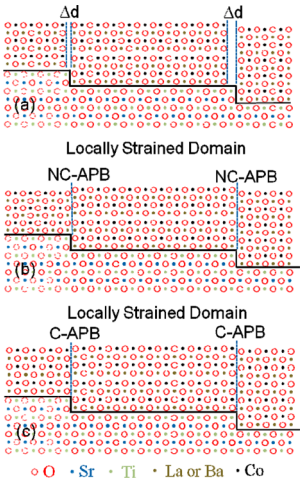


**Figure 6.** Thin-film/substrate mismatch in the epitaxial LaBCO film grown on the vicinal (001) $SrTiO_3$ substrates with low miscut angle. (a) The generation of the "residual mismatching gap" at the end of the step terrace. (b) The formation of nonconservative antiphase domain boundary. (c) The formation of locally strained domain with conservative antiphase domain boundary induced by the "residual mismatching gap".

gap, it is highly impossible to form a nonconservative antiphase domain boundary at the end of the substrate terrace, since a huge amount of interface strain energy will be generated due to the same charge repulsion at the domain boundary and interface. Therefore, it is highly likely that the residual matching gap will be released via the formation of locally strained domain, which will result in the tensile strain over the interface and the compressive strain along the out-of-plane direction. However, the local strain can significantly alter the epitaxial quality and their physical properties.[24] These can be seen from strong transport electron scattering behavior, as seen in Figure 3, where the resistance behavior for the film on the 0.5° miscut surface is more semiconductor-like, rather than the semimetallic behavior found for the films on the 3.0° and 5.0° vicinal surfaces. This might be considered as resulting from the strain-induced distortion of the $CoO_6$ octahedral structure and change the Co−O bond length and Co−O−Co bond angles, causing the reduction of the charge carriers hopping.

The MR for the film on the 0.5° miscut surface is larger than the other two samples, which mainly result from the local strain induced by the residual mismatching gap and the competition between the AFM and FM states. Under the application of magnetic field, the disordered scattering rate from local strain lattice structures will be decreased and the conductivity increased, resulting in the largest negative MR value. On the other hand, the 0.5° miscut films have a smaller magnetic moment than the other two samples (Figure 5), indicating that the 0.5° miscut film has a greater AFM domain under the local strain conditions. Therefore, when the external magnetic field is applied, the subtle balance between AFM and FM phases will be changed to induce the large MR value.

## CONCLUSION

In summary, high-quality LaBCO thin films are epitaxially grown on the (001) $SrTiO_3$ substrates with different miscut angles by pulsed laser ablation. Transport property studies show that the 3.0° and 5.0° miscut films have a typical semimetal behavior due to their single domain and small lattice misfit strain. The 0.5° film shows a semiconductor behavior resulting from the formation of the locally strained domain structures induced from the mismatch of the substrate step terrace dimension and the epitaxial film, which induce a larger MR value of 34% at 60 K.

## AUTHOR INFORMATION

### Corresponding Author

*E-mail: cl.chen@utsa.edu.

### Notes

The authors declare no competing financial interest.

## ACKNOWLEDGMENTS

This research was partially supported by the Department of Energy (under Award No. DE-FE0003780), the National Science Foundation (under Award No. NSF-NIRT-0709293), the State of Texas through the Texas Center for Superconductivity at the University of Houston, and the Natural Science Foundation of China (under No. 11028409). C.M. and M.L. would like to acknowledge the support from the "China Scholarship Council" for their Ph.D. studies at UTSA.

## REFERENCES

(1) Senarisrodriguez, M. A.; Goodenough, J. B. *J. Solid State Chem.* **1995**, *118* (2), 323−336.
(2) Luo, G. P.; Wang, Y. S.; Chen, S. Y.; Heilman, A. K.; Chen, C. L.; Chu, C. W.; Liou, Y.; Ming, N. B. *Appl. Phys. Lett.* **2000**, *76* (14), 1908−1910.
(3) Yang, Y. L.; Chen, C. L.; Chen, S. Y.; Chu, C. W.; Jacobson, A. J. *J. Electrochem. Soc.* **2000**, *147* (11), 4001−4007.
(4) Akahoshi, D.; Ueda, Y. *J. Solid State Chem.* **2001**, *156* (2), 355−363.
(5) Yang, Y. M. L.; Jacobson, A. J.; Chen, C. L.; Luo, G. P.; Ross, K. D.; Chu, C. W. *Appl. Phys. Lett.* **2001**, *79* (6), 776−778.
(6) Podlesnyak, A.; Streule, S.; Mesot, J.; Medarde, M.; Pomjakushina, E.; Conder, K.; Tanaka, A.; Haverkort, M. W.; Khomskii, D. I. *Phys. Rev. Lett.* **2006**, *97* (24), 247208.
(7) Kozlenko, D. P.; Jirak, Z.; Golosova, N. O.; Savenko, B. N. *Eur. Phys. J. B* **2009**, *70* (3), 327−334.
(8) Zhang, Y. M.; Whangbo, M. H. *Inorg. Chem.* **2011**, *50* (21), 10643−10647.
(9) Yuan, Z.; Liu, J.; Chen, C. L.; Wang, C. H.; Luo, X. G.; Chen, X. H.; Kim, G. T.; Huang, D. X.; Wang, S. S.; Jacobson, A. J.; Donner, W. *Appl. Phys. Lett.* **2007**, *90* (21), 212111.
(10) Nakajima, T.; Ichihara, M.; Ueda, Y. *J. Phys. Soc. Jpn.* **2005**, *74* (5), 1572−1577.
(11) Rautama, E. L.; Boullay, P.; Kundu, A. K.; Caignaert, V.; Pralong, V.; Karppinen, M.; Raveau, B. *Chem. Mater.* **2008**, *20* (8), 2742−2750.
(12) Rautama, E. L.; Caignaert, V.; Boullay, P.; Kundu, A. K.; Pralong, V.; Karppinen, M.; Ritter, C.; Raveau, B. *Chem. Mater.* **2009**, *21* (1), 102−109.
(13) He, J.; Jiang, J. C.; Liu, J.; Liu, M.; Collins, G.; Ma, C. R.; Chen, C. L.; Meletis, E. I. *Thin Solid Films* **2011**, *519* (13), 4371−4376.
(14) Liu, J.; Collins, G.; Liu, M.; Chen, C. L.; Jiang, J. C.; Meletis, E. I.; Zhang, Q. Y.; Dong, C. A. *Appl. Phys. Lett.* **2010**, *97* (9), 094101.
(15) Liu, J.; Liu, M.; Collins, G.; Chen, C. L.; Jiang, X. N.; Gong, W. Q.; Jacobson, A. J.; He, J.; Jiang, J. C.; Meletis, E. I. *Chem. Mater.* **2010**, *22* (3), 799−802.
(16) Liu, M.; Liu, J.; Collins, G.; Ma, C. R.; Chen, C. L.; He, J.; Jiang, J. C.; Meletis, E. I.; Jacobson, A. J.; Zhang, Q. Y. *Appl. Phys. Lett.* **2010**, *96* (13), 132106.
(17) Liu, M.; Ma, C. R.; Liu, J.; Collins, G.; Chen, C. L.; He, J.; Jiang, J. C.; Meletis, E. I.; Sun, L.; Jacobson, A. J.; Whangbo, M. H. *ACS Appl. Mater. Interfaces* **2012**, *4* (10), 5524−5528.

(18) Ma, C. R.; Liu, M.; Collins, G.; Liu, J.; Zhang, Y. M.; Chen, C. L.; He, J.; Jiang, J. C.; Meletis, E. I. *Appl. Phys. Lett.* **2012**, *101* (2), 021602.
(19) Chen, C. L.; Shen, J.; Chen, S. Y.; Luo, G. P.; Chu, C. W.; Miranda, F. A.; Van Keuls, F. W.; Jiang, J. C.; Meletis, E. I.; Chang, H. Y. *Appl. Phys. Lett.* **2001**, *78* (5), 652−654.
(20) Jiang, J. C.; Lin, Y.; Chen, C. L.; Chu, C. W.; Meletis, E. I. *J. Appl. Phys.* **2002**, *91* (5), 3188−3192.
(21) Lin, Y.; Chen, X.; Liu, S. W.; Chen, C. L.; Lee, J. S.; Li, Y.; Jia, Q. X.; Bhalla, A. *Appl. Phys. Lett.* **2004**, *84* (4), 577−579.
(22) Liu, S. W.; Lin, Y.; Weaver, J.; Donner, W.; Chen, X.; Chen, C. L.; Jiang, J. C.; Meletis, E. I.; Bhalla, A. *Appl. Phys. Lett.* **2004**, *85* (15), 3202−3204.
(23) Huang, D. X.; Chen, C. L.; Jacobson, A. J. *J. Appl. Phys.* **2005**, *97* (4), 043506.
(24) Lu, H. L.; Zhang, C. D.; Guo, H. M.; Gao, H. J.; Liu, M.; Liu, J. A.; Collins, G.; Chen, C. L. *ACS Appl. Mater. Interfaces* **2010**, *2* (9), 2496−2499.
(25) Chen, C. L.; Cao, Y.; Huang, Z. J.; Jiang, Q. D.; Zhang, Z.; Sun, Y. Y.; Kang, W. N.; Dezaneti, L. M.; Chu, W. K.; Chu, C. W. *Appl. Phys. Lett.* **1997**, *71* (8), 1047−1049.
(26) Canadell, E.; Whangbo, M. H. *Inorg. Chem.* **1990**, *29* (7), 1398−1401.
(27) Gourdon, O.; Jeanneau, E.; Evain, M.; Jobic, S.; Brec, R. *J. Solid State Chem.* **2001**, *162* (1), 103−112.
(28) Kundu, A. K.; Rautama, E. L.; Boullay, P.; Caignaert, V.; Pralong, V.; Raveau, B. *Phys. Rev. B* **2007**, *76* (18), 184432.
(29) Kundu, A. K.; Raveau, B.; Caignaert, V.; Rautama, E. L.; Pralong, V. *J. Phys.: Condens. Matter* **2009**, *21* (5), 056007.
(30) Taskin, A. A.; Lavrov, A. N.; Ando, Y. *Phys. Rev. B* **2005**, *71* (13), 134414.
(31) Taskin, A. A.; Lavrov, A. N.; Ando, Y. *Phys. Rev. B* **2006**, *73* (12), 121101.
(32) Chen, C. L.; Tsong, T. T. *Phys. Rev. Lett.* **1990**, *64* (26), 3147−3150.
(33) Chen, C. L.; Tsong, T. T. *Phys. Rev. B* **1990**, *41* (18), 12403−12412.
(34) Rao, R. A.; Gan, Q.; Eom, C. B. *Appl. Phys. Lett.* **1997**, *71* (9), 1171−1173.